

C-LoRA: Continual Low-Rank Adaptation for Pre-trained Models

Xin Zhang, Liang Bai, Xian Yang, Jiye Liang *Fellow, IEEE*

Abstract—Low-Rank Adaptation (LoRA) is an efficient fine-tuning method that has been extensively applied in areas such as natural language processing and computer vision. Existing LoRA fine-tuning approaches excel in static environments but struggle in dynamic learning due to reliance on multiple adapter modules, increasing overhead and complicating inference. We propose Continual Low-Rank Adaptation (C-LoRA), a novel extension of LoRA for continual learning. C-LoRA uses a learnable routing matrix to dynamically manage parameter updates across tasks, ensuring efficient reuse of learned subspaces while enforcing orthogonality to minimize interference and forgetting. Unlike existing approaches that require separate adapters for each task, C-LoRA enables an integrated approach for task adaptation, achieving both scalability and parameter efficiency in sequential learning scenarios. C-LoRA achieves state-of-the-art accuracy and parameter efficiency on benchmarks while providing theoretical insights into its routing matrix’s role in retaining and transferring knowledge, establishing a scalable framework for continual learning.

Index Terms—Continual Learning, Catastrophic Forgetting, Low-Rank Adapter, Pre-trained Model.

I. INTRODUCTION

LOW-RANK Adaptation (LoRA) [1] is a parameter-efficient fine-tuning method that adapts large-scale pre-trained models to downstream tasks by introducing low-rank matrices to update a small subset of parameters while keeping the core pre-trained weights frozen. This approach preserves the general knowledge captured during pre-training, reduces computational and storage costs, and mitigates the risk of overfitting by limiting updates to task-specific components [2]. LoRA has proven highly effective in fields such as natural language processing and computer vision, where large models are commonly deployed for diverse and evolving applications [3]–[6].

Despite its advantages, existing LoRA frameworks are optimized for static environments with fixed datasets and tasks. In dynamic and evolving scenarios, such as continual learning, traditional LoRA methods face limitations. Continual learning requires a model to learn from a continuous stream of tasks or data, accumulating knowledge over time without forgetting previously acquired information [7]. The goal of continual learning is to overcome catastrophic forgetting, where a model loses its ability to recall and perform well on earlier tasks while adapting to new ones, resulting in a decrease to effectively

transfer and accumulate knowledge and leading to a decline in performance [8]–[11]. New adapter modules are typically introduced for each task to prevent interference, resulting in Linear growth in parameters and computational overhead [3]–[6]. This approach complicates inference, as selecting the appropriate adapter becomes increasingly challenging with the growing number of tasks.

To address these limitations, we propose Continual Low-Rank Adaptation (C-LoRA), an extension of LoRA designed for dynamic environments. C-LoRA introduces a learnable routing matrix \mathcal{R} , which decomposes into components managing both previous and new task parameters. By enforcing orthogonality constraints, C-LoRA reduces interference between tasks, mitigating catastrophic forgetting and enhancing the model’s ability to retain prior knowledge. This design allows for parameter-efficient continual learning by leveraging shared low-rank subspaces across tasks, reducing the need for extensive storage and computational resources. The contributions of this work are listed as follows:

- C-LoRA addressed the question, “Can One LoRA Replace Multiple LoRAs?” and shed light on the forgetting mechanisms between the routing matrix \mathcal{R} and the LoRA subspace.
- C-LoRA subspace design and orthogonality constraint eliminate interference from new task on old tasks, mitigating catastrophic forgetting and enhancing the model’s ability to retain prior knowledge.
- Experimental results show that C-LoRA outperforms existing state-of-the-art continual learning methods across multiple datasets.

II. RELATED WORK

Continual Learning (CL) requires model to continuously learn and recognize new classes without forgetting what it has previously learned [12]–[17]. Traditional CL methods can be grouped into four main approaches: replay-based, knowledge distillation, model architecture, and regularization-based methods. Replay-based methods [18]–[24] involve store a subset of data from previous classes and replay them during training on new classes to preserve existing knowledge. Knowledge distillation methods [25]–[29] retain information from previously learned classes by using auxiliary loss functions that ensure the outputs of the old model is preserved while learning new classes. Model architecture methods [6], [30]–[33] modify the network structure to integrate new classes by designing specialized parameter modules for each stages, ensuring that the learning of new classes doesn’t interfere with previously acquired knowledge. Regularization-based methods [25], [27], [34]–[37] impose constraints on the model’s parameters to

Xin Zhang, Liang Bai and Jiye Liang are with Institute of Intelligent Information Processing, Shanxi University, Taiyuan, 030006, China (Corresponding author: Liang Bai)
Email: 202322407065@email.sxu.edu.cn, bailiang@sxu.edu.cn, ljj@sxu.edu.cn

Xian Yang is with Alliance Manchester Business School, The University of Manchester, Manchester, M13 9PL, UK
Email: xian.yang@manchester.ac.uk

prevent substantial changes that could lead to forgetting, thereby maintaining the integrity of important weights.

LoRA [1] is an efficient model fine-tuning method. Instead of fine-tuning the entire pre-trained model, LoRA fine-tunes specific submodules of the pre-trained model by inserting low-rank matrices. Traditional LoRA performs well in static task environments, where the tasks and data remain fixed during training [38]–[40]. In continual learning settings, however, the traditional LoRA method faces challenges, particularly in handling the arrival of new tasks while retaining knowledge from previous ones to prevent catastrophic forgetting. To address this challenge, a prevalent strategy involves combining multiple LoRA modules, each responsible for handling specific tasks within the input data [4], [41], [42]. The Mixture of Experts (MoE) [43], [44] framework integrates multiple expert networks and assigns tasks through a gating mechanism, thereby enhancing the model’s performance across diverse tasks. Inspired by this, MoE-LoRA [3] introduces a mixture of experts model to allocate and select LoRA modules, reducing conflicts between new and existing tasks. Additionally, infLoRA [42] uses independent LoRA submodules for each new task and employs regularization techniques to minimize interference between new and old tasks. EASE [4] addresses data distribution changes by storing prototypes of each task-specific subspace and adopting a semantic-guided prototype augmentation strategy. Online-LoRA [41] implements an online weight regularization strategy that automatically identifies changes in data distribution to reduce forgetting. However, these methods rely on multiple LoRA modules, leading to a linear increase in parameter and computational overhead, and the challenge of effectively integrating all LoRA modules during inference.

III. METHODOLOGY

In this chapter, we define the problem of Continual Learning and address the core question—“Can a single LoRA replace multiple LoRAs?” we propose a novel learnable matrix \mathcal{R} that dynamically controls how parameter subspaces are activated and updated, with its element magnitudes influencing the degree of forgetting. Excessive updates to shared subspaces risk overwriting prior knowledge. Based on this analysis, we propose the C-LoRA architecture and its training paradigm.

A. Preliminaries

LoRA [1] is a parameter-efficient fine-tuning method that adapts large-scale pre-trained models to specific tasks by introducing low-rank matrices. For a pre-trained linear layer $\mathbf{W}_0 \in \mathbb{R}^{d \times k}$, LoRA applies a low-rank update $\Delta \mathbf{W} = \mathbf{A}\mathbf{B}$, where $\mathbf{A} \in \mathbb{R}^{d \times r}$ and $\mathbf{B} \in \mathbb{R}^{r \times k}$ are trainable matrices with rank $r \ll \min(d, k)$. The updated weight for task t is:

$$\mathbf{W}_t = \mathbf{W}_0 + \Delta \mathbf{W}_t = \mathbf{W}_0 + \mathbf{A}_t \mathbf{B}_t, \quad (1)$$

where \mathbf{A}_t and \mathbf{B}_t are the task-specific low-rank matrices. By keeping \mathbf{W}_0 frozen and only updating \mathbf{A}_t and \mathbf{B}_t , LoRA achieves significant parameter efficiency compared to full fine-tuning.

In *continual learning* scenarios, a model must learn a sequence of tasks $\{\mathcal{T}_1, \mathcal{T}_2, \dots, \mathcal{T}_T\}$ without forgetting prior knowledge. To prevent task interference, existing LoRA-based methods [4], [41], [42] introduce a separate low-rank update $\Delta \mathbf{W}_t = \mathbf{A}_t \mathbf{B}_t$ for each task \mathcal{T}_t . As a result, the model maintains a collection of task-specific parameters:

$$\{(\mathbf{A}_1, \mathbf{B}_1), (\mathbf{A}_2, \mathbf{B}_2), \dots, (\mathbf{A}_T, \mathbf{B}_T)\}. \quad (2)$$

However, this approach has two major limitations: 1) **Parameter Growth**: The number of LoRA modules grows linearly with the number of tasks, leading to significant storage and computational overhead. 2) **Inference Complexity**: During inference, selecting the correct adapter $(\mathbf{A}_T, \mathbf{B}_T)$ for a given task \mathcal{T}_t becomes increasingly cumbersome as the number of tasks T grows. These challenges motivate the need for an approach that avoids parameter proliferation while retaining knowledge across tasks. Specifically, we pose the question: **Can a single LoRA replace multiple LoRAs in continual learning?** This question forms the foundation of our proposed approach, introduced in the next section.

B. Continual Low-Rank Adaptation

To address the limitations of existing LoRA-based methods in continual learning, we propose *Continual Low-Rank Adaptation (C-LoRA)*. The core idea of C-LoRA is to replace multiple task-specific LoRA modules with a single adaptable LoRA mechanism, managed by a learnable routing matrix \mathcal{R} .

The routing matrix \mathcal{R} dynamically controls how parameter subspaces are activated and updated for each task. Formally, for a pre-trained linear layer with weights \mathbf{W}_0 , the task-specific adaptation in C-LoRA is expressed as:

$$\mathbf{W}_t = \mathbf{W}_0 + \Delta \mathbf{W}_t, \quad \Delta \mathbf{W}_t = \mathbf{A} \mathcal{R} \mathbf{B}, \quad (3)$$

where $\mathbf{A} \in \mathbb{R}^{d \times r}$ and $\mathbf{B} \in \mathbb{R}^{r \times k}$ are low-rank matrices shared across tasks, and $\mathcal{R} \in \mathbb{R}^{r \times r}$ is the learnable routing matrix that determines the dynamic contribution of different subspaces.

As illustrated in Figure 1, the routing matrix \mathcal{R} generalizes the concept of a MoE [3] by integrating contributions from multiple subspaces into a single low-rank adaptation framework. In MoE, each expert is associated with a weight w_i and distinct low-rank projections $\mathbf{A}_i \in \mathbb{R}^{d \times \frac{r}{h}}$ and $\mathbf{B}_i \in \mathbb{R}^{\frac{r}{h} \times k}$, with the output aggregated as:

$$\sum_{i=1}^h w_i \mathbf{A}_i \mathbf{B}_i. \quad (4)$$

C-LoRA simplifies this structure by combining the subspaces into shared low-rank matrices \mathbf{A} and \mathbf{B} and using \mathcal{R} to represent the routing mechanism:

$$\mathcal{R} = \text{diag}(w_1 \mathbf{I}_{\frac{r}{h}}, w_2 \mathbf{I}_{\frac{r}{h}}, \dots, w_h \mathbf{I}_{\frac{r}{h}}), \quad (5)$$

where $w_i \in \mathbb{R}$ are the weights associated with subspaces, $\mathbf{I}_{\frac{r}{h}}$ is an identity matrix of size $\frac{r}{h} \times \frac{r}{h}$, and h represents the number of subspaces. This design allows efficient sharing of subspaces while isolating task-specific updates.

During training, \mathcal{R} is decomposed into \mathcal{R}_{old} and \mathcal{R}_{δ} , where \mathcal{R}_{old} captures shared knowledge from previous tasks, and \mathcal{R}_{δ}

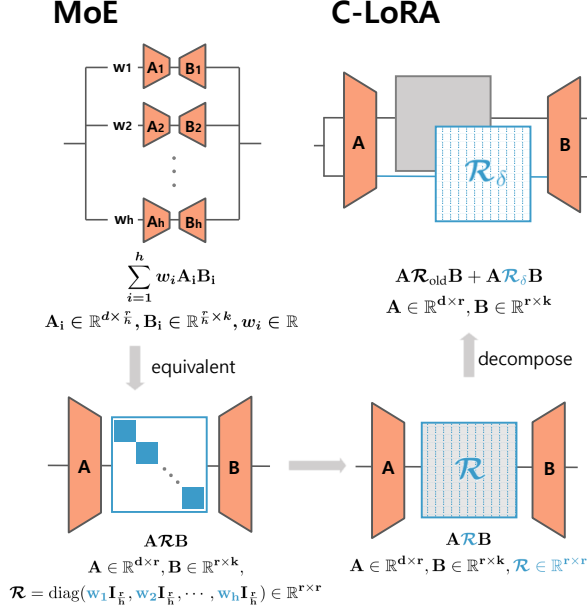


Fig. 1. Comparison of MoE and proposed C-LoRA architecture. We extend the equivalent form of MoE and decompose the routing matrix \mathcal{R} into two parts: \mathcal{R}_{old} and \mathcal{R}_δ , where \mathcal{R}_{old} does not participate in gradient computation during training.

introduces task-specific updates for the current task. Orthogonality constraints are applied to \mathcal{R}_δ , ensuring that updates for new tasks do not interfere with shared knowledge. As highlighted in Figure 1, this decomposition decouples the shared and task-specific components, with \mathcal{R}_{old} remaining frozen during gradient computation, ensuring efficient adaptation.

By leveraging the routing matrix \mathcal{R} , C-LoRA achieves a mechanism for continual learning that consolidates multiple task-specific LoRA modules into a single adaptable framework. This design preserves previously learned information while enabling scalable and efficient adaptation to new tasks. In the following sections, we provide detailed theoretical insights into \mathcal{R} and describe the training paradigm of C-LoRA.

C. The Role of \mathcal{R} in Forgetting Control

In this subsection, we further analyze the role of matrix \mathcal{R} during the forward and backward propagation processes, establishing the theoretical foundation for our C-LoRA architecture. For clarity, we focus on a linear segment of the network, represented by $\mathbf{y} = \mathbf{x}\mathbf{W}$, where the weight matrix \mathbf{W} is determined by $\mathbf{W} = \mathbf{A}\mathcal{R}\mathbf{B}$. Since non-linear activation functions only perform non-linear transformations on the results of matrix multiplications and do not affect the low-rank decomposition of the weight matrices themselves, they are omitted here.

Representation of \mathbf{A} , \mathbf{B} , \mathcal{R} : Specifically, $\mathbf{A} \in \mathbb{R}^{d \times r}$ is a matrix composed of r column vectors $[\mathbf{a}_1, \mathbf{a}_2, \dots, \mathbf{a}_r]$, each $\mathbf{a}_i \in \mathbb{R}^d$. $\mathbf{B} \in \mathbb{R}^{r \times k}$ consists of r row vectors $[\mathbf{b}_1^\top, \mathbf{b}_2^\top, \dots, \mathbf{b}_r^\top]$, each $\mathbf{b}_j^\top \in \mathbb{R}^k$. Matrix $\mathcal{R} \in \mathbb{R}^{r \times r}$ contains elements r_{ij} . We can express \mathbf{A} , \mathcal{R} , and \mathbf{B} as follows:

$$\mathbf{A} = \sum_{i=1}^r \mathbf{a}_i \mathbf{e}_i^\top, \quad \mathcal{R} = \sum_{i=1}^r \sum_{j=1}^r r_{ij} \mathbf{e}_i \mathbf{e}_j^\top, \quad \mathbf{B} = \sum_{j=1}^r \mathbf{e}_j \mathbf{b}_j^\top, \quad (6)$$

where $\mathbf{e}_i \in \mathbb{R}^r$ is the i -th standard basis vector with a 1 in the i -th position, and all other entries are 0.

Forward Propagation with \mathcal{R} : During the forward propagation process, each element r_{ij} in matrix \mathcal{R} determines the contribution of the i -th column of \mathbf{A} and the j -th row of \mathbf{B} to the feature transformation. Specifically,

$$\begin{aligned} \mathbf{W} &= \left(\sum_{i=1}^r \mathbf{a}_i \mathbf{e}_i^\top \right) \left(\sum_{i=1}^r \sum_{j=1}^r r_{ij} \mathbf{e}_i \mathbf{e}_j^\top \right) \left(\sum_{j=1}^r \mathbf{e}_j \mathbf{b}_j^\top \right) \\ &= \sum_{i=1}^r \sum_{j=1}^r r_{ij} \mathbf{a}_i \mathbf{b}_j^\top. \end{aligned} \quad (7)$$

Meaning that each non-zero element r_{ij} in \mathcal{R} activates the i -th column vector \mathbf{a}_i of \mathbf{A} and the j -th row vector \mathbf{b}_j^\top of \mathbf{B} to varying degrees. Larger element values indicate a higher importance of the corresponding subspace in the current task.

Backward Propagation and Gradient Updates: During the backward propagation phase, matrix \mathcal{R} plays a pivotal role in determining which parameters receive gradients and are subsequently updated. Specifically, Let \mathbf{G} represent the gradient with respect to \mathbf{W} :

$$\mathbf{G} = \frac{\partial \mathbf{y}}{\partial \mathbf{W}}. \quad (8)$$

Consequently, the gradients of \mathbf{A} and \mathbf{B} are given by:

$$\begin{aligned} \frac{\partial \mathbf{y}}{\partial \mathbf{A}} &= \mathbf{G} \mathbf{B}^\top \mathcal{R}^\top = \mathbf{G} \left(\sum_{i=1}^r \sum_{j=1}^r r_{ij} \mathbf{b}_j \mathbf{e}_j^\top \right), \\ \frac{\partial \mathbf{y}}{\partial \mathbf{B}} &= \mathcal{R}^\top \mathbf{A}^\top \mathbf{G} = \left(\sum_{i=1}^r \sum_{j=1}^r r_{ij} \mathbf{e}_j \mathbf{a}_i^\top \right) \mathbf{G}. \end{aligned} \quad (9)$$

Furthermore, the gradients of the i -th column of \mathbf{A} and the j -th row of \mathbf{B} can be expressed as:

$$\left(\frac{\partial \mathbf{y}}{\partial \mathbf{A}} \right)_{:,i} = \mathbf{G} \sum_{j=1}^r r_{ij} \mathbf{b}_j, \quad \left(\frac{\partial \mathbf{y}}{\partial \mathbf{B}} \right)_{j,:} = \sum_{i=1}^r r_{ij} \mathbf{a}_i^\top \mathbf{G}. \quad (10)$$

These equations illustrate that each non-zero element r_{ij} in \mathcal{R} governs the gradient updates of the corresponding columns in \mathbf{A} and rows in \mathbf{B} . The value of r_{ij} not only influences the representation capacity for the current task but also directly controls the extent of interference with parameters from previous tasks. A larger r_{ij} value indicates a higher importance of the corresponding subspace in the old task, making it more susceptible to overwriting or modifying previously acquired knowledge when learning new tasks. This, in turn, exacerbates the forgetting of knowledge from prior tasks.

Decomposition of \mathcal{R} : To balance the conflict between newly acquired and previously learned knowledge, we propose decomposing matrix \mathcal{R} into two components:

$$\mathcal{R} = \mathcal{R}_{old} + \mathcal{R}_\delta \quad (11)$$

Here, \mathcal{R}_{old} accumulates the \mathcal{R}_δ values learned from previous tasks, and preserves the importance of parameters in the subspace of old tasks. \mathcal{R}_δ is dedicated to the incremental learning of new tasks. Specifically, \mathcal{R}_δ is initialized as a near-zero matrix when a new task arrives, ensuring that learning new tasks minimally impacts the parameters of old tasks. This decomposition mechanism ensures that the critical parameters of old tasks are not significantly affected by the training of new tasks, while allowing the model to flexibly adjust and learn in new tasks. Specifically, during training, we isolate the parameter updates of the \mathcal{R}_{old} component, concentrating the majority of updates on the \mathcal{R}_δ component. This approach protects the subspace of key parameters for old tasks from excessive interference by new tasks. After updating, our network can be expressed as:

$$\mathbf{y}' = \mathbf{x}\mathbf{W}' \quad \text{where} \quad \mathbf{W}' = \phi(\mathbf{A}\mathcal{R}_{\text{old}}\mathbf{B}) + \mathbf{A}\mathcal{R}_\delta\mathbf{B}, \quad (12)$$

where $\phi(\cdot)$ denote that gradients are not computed for this operation. This ensures that the model leverages the knowledge from old tasks while incrementally learning new tasks, significantly mitigating the phenomenon of catastrophic forgetting.

Theoretical Validation: To further validate the effectiveness of this decomposition design, we present the following theorem:

Theorem 3.1. *Let \mathcal{R} be divided into $\mathcal{R}_{\text{old}} + \mathcal{R}_\delta$ with \mathcal{R}_{old} fixed and \mathcal{R}_δ trainable. If:*

1. $\mathcal{R}_{\text{old}}^\top \mathcal{R}_\delta$ is positive definite.
2. $\mathbf{B}\mathbf{G}^\top \neq 0$ and $\mathbf{G}^\top \mathbf{A} \neq 0$.

Then, the upper bounds on the parameter changes of \mathbf{A} and \mathbf{B} using the decomposed routing \mathcal{R} are tighter compared to directly training \mathcal{R} . Specifically:

$$\left\| \frac{\partial \mathbf{y}}{\partial \mathbf{A}} \right\|_F^2 > \left\| \frac{\partial \mathbf{y}'}{\partial \mathbf{A}} \right\|_F^2, \quad \left\| \frac{\partial \mathbf{y}}{\partial \mathbf{B}} \right\|_F^2 > \left\| \frac{\partial \mathbf{y}'}{\partial \mathbf{B}} \right\|_F^2. \quad (13)$$

Proof of Theorem 3.1. Let $\mathbf{G} = \frac{\partial \mathbf{y}}{\partial \mathbf{W}}$. represent the gradient with respect to the weight matrix. The partial derivatives of \mathbf{y} and \mathbf{y}' with respect to \mathbf{A} are given by:

$$\begin{aligned} \frac{\partial \mathbf{y}}{\partial \mathbf{A}} &= \mathbf{G}\mathbf{B}^\top \mathcal{R}^\top = \mathbf{G}(\mathcal{R}_{\text{old}} + \mathcal{R}_\delta)^\top \mathbf{B}^\top, \\ \frac{\partial \mathbf{y}'}{\partial \mathbf{A}} &= \mathbf{G}\mathcal{R}_\delta^\top \mathbf{B}^\top. \end{aligned} \quad (14)$$

Computing the squared Frobenius norm difference, we have:

$$\begin{aligned} \left\| \frac{\partial \mathbf{y}}{\partial \mathbf{A}} \right\|_F^2 - \left\| \frac{\partial \mathbf{y}'}{\partial \mathbf{A}} \right\|_F^2 &= \left\| \mathbf{G}\mathbf{B}^\top (\mathcal{R}_{\text{old}} + \mathcal{R}_\delta)^\top \right\|^2 - \left\| \mathbf{G}\mathbf{B}^\top \mathcal{R}_\delta^\top \right\|^2 \\ &= \text{Tr} \left[(\mathbf{G}\mathbf{B}^\top (\mathcal{R}_{\text{old}} + \mathcal{R}_\delta)^\top)^\top (\mathbf{G}\mathbf{B}^\top (\mathcal{R}_{\text{old}} + \mathcal{R}_\delta)^\top) \right] \\ &\quad - \text{Tr} \left[(\mathbf{G}\mathbf{B}^\top \mathcal{R}_\delta^\top)^\top (\mathbf{G}\mathbf{B}^\top \mathcal{R}_\delta^\top) \right] \\ &= \text{Tr} \left[(\mathcal{R}_{\text{old}} + \mathcal{R}_\delta) \mathbf{B}\mathbf{G}^\top \mathbf{G}\mathbf{B}^\top (\mathcal{R}_{\text{old}} + \mathcal{R}_\delta)^\top \right] \\ &\quad - \text{Tr} \left[\mathcal{R}_\delta \mathbf{B}\mathbf{G}^\top \mathbf{G}\mathbf{B}^\top \mathcal{R}_\delta^\top \right] \\ &= \text{Tr} \left[\mathcal{R}_{\text{old}} \mathbf{B}\mathbf{G}^\top \mathbf{G}\mathbf{B}^\top \mathcal{R}_{\text{old}}^\top \right] + 2\text{Tr} \left[\mathcal{R}_\delta \mathbf{B}\mathbf{G}^\top \mathbf{G}\mathbf{B}^\top \mathcal{R}_{\text{old}}^\top \right] \\ &= \text{Tr} \left[(\mathcal{R}_{\text{old}}^\top \mathcal{R}_{\text{old}} + 2\mathcal{R}_{\text{old}}^\top \mathcal{R}_\delta) (\mathbf{B}\mathbf{G}^\top \mathbf{G}\mathbf{B}^\top) \right] \\ &> 0 \end{aligned} \quad (15)$$

where the last inequality holds due to the positive definiteness of $\mathcal{R}_{\text{old}}^\top \mathcal{R}_\delta$ and $\mathbf{B}\mathbf{G}^\top \neq 0$.

Similarly, the partial derivatives of \mathbf{y} and \mathbf{y}' with respect to \mathbf{B} are given by:

$$\begin{aligned} \frac{\partial \mathbf{y}}{\partial \mathbf{B}} &= \mathcal{R}^\top \mathbf{A}^\top \mathbf{G} = (\mathcal{R}_{\text{old}} + \mathcal{R}_\delta)^\top \mathbf{A}^\top \mathbf{G}, \\ \frac{\partial \mathbf{y}'}{\partial \mathbf{B}} &= \mathcal{R}_\delta^\top \mathbf{A}^\top \mathbf{G}. \end{aligned} \quad (16)$$

Calculating the squared Frobenius norm difference, we have:

$$\begin{aligned} \left\| \frac{\partial \mathbf{y}}{\partial \mathbf{B}} \right\|_F^2 - \left\| \frac{\partial \mathbf{y}'}{\partial \mathbf{B}} \right\|_F^2 &= \left\| (\mathcal{R}_{\text{old}} + \mathcal{R}_\delta)^\top \mathbf{A}^\top \mathbf{G} \right\|^2 - \left\| \mathcal{R}_\delta^\top \mathbf{A}^\top \mathbf{G} \right\|^2 \\ &= \text{Tr} \left[((\mathcal{R}_{\text{old}} + \mathcal{R}_\delta)^\top \mathbf{A}^\top \mathbf{G})^\top ((\mathcal{R}_{\text{old}} + \mathcal{R}_\delta)^\top \mathbf{A}^\top \mathbf{G}) \right] \\ &\quad - \text{Tr} \left[(\mathcal{R}_\delta^\top \mathbf{A}^\top \mathbf{G})^\top (\mathcal{R}_\delta^\top \mathbf{A}^\top \mathbf{G}) \right] \\ &= \text{Tr} \left[\mathbf{G}^\top \mathbf{A} (\mathcal{R}_{\text{old}} + \mathcal{R}_\delta) (\mathcal{R}_{\text{old}} + \mathcal{R}_\delta)^\top \mathbf{A}^\top \mathbf{G} \right] \\ &\quad - \text{Tr} \left[\mathbf{G}^\top \mathbf{A} \mathcal{R}_\delta \mathcal{R}_\delta^\top \mathbf{A}^\top \mathbf{G} \right] \\ &= \text{Tr} \left[\mathbf{G}^\top \mathbf{A} \mathcal{R}_{\text{old}} \mathcal{R}_{\text{old}}^\top \mathbf{A}^\top \mathbf{G} \right] + 2\text{Tr} \left[\mathbf{G}^\top \mathbf{A} \mathcal{R}_\delta \mathcal{R}_{\text{old}}^\top \mathbf{A}^\top \mathbf{G} \right] \\ &= \text{Tr} \left[(\mathcal{R}_{\text{old}} \mathcal{R}_{\text{old}}^\top + 2\mathcal{R}_\delta \mathcal{R}_{\text{old}}^\top) (\mathbf{A}^\top \mathbf{G} \mathbf{G}^\top \mathbf{A}) \right] \\ &> 0 \end{aligned} \quad (17)$$

where the last inequality holds due to the positive definiteness of $\mathcal{R}_{\text{old}}^\top \mathcal{R}_\delta$ and $\mathbf{G}^\top \mathbf{A} \neq 0$. \square

This theorem demonstrates that by decomposing \mathcal{R} into $\mathcal{R}_{\text{old}} + \mathcal{R}_\delta$ and isolating the gradient updates of the \mathcal{R}_{old} component during training, the interference of new tasks with the critical parameters of old tasks is reduced. This supports the feasibility of our proposed method.

D. Implementation Details: C-LoRA in ViT Application

Building on our C-LoRA approach, this section details its application to Vision Transformers (ViT) [45] for efficient continual learning. ViTs have emerged as a powerful architecture for image recognition tasks due to their ability to model long-range dependencies using self-attention mechanisms. Each layer of a ViT consists of two main components: the multi-head self-attention (MSA) block and the multi-layer perceptron (MLP) block. While the MSA block captures contextual

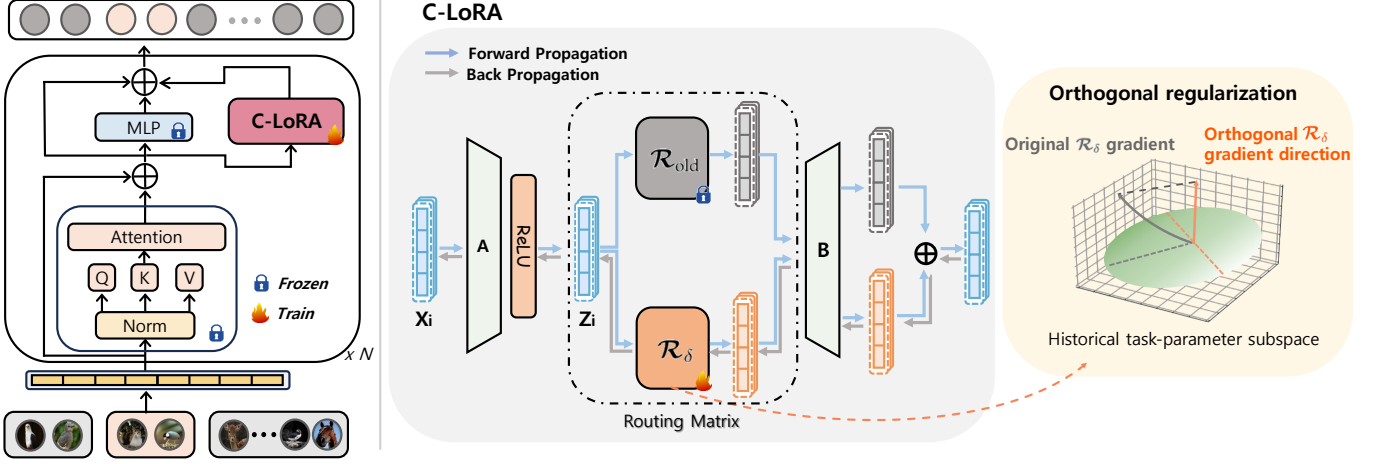


Fig. 2. Illustration of the Proposed Model. **Left:** Vision Transformer (ViT) integrated with the C-LoRA module, where the adapter and local classifier are incrementally trained in each session. **Right:** Proposed architecture mitigates catastrophic forgetting by decoupling \mathcal{R} to constrain updates within the parameter space of previous tasks and enforcing orthogonality between \mathcal{R} updates and the low-rank parameter space of past tasks.

relationships among input tokens, the MLP block processes feature embeddings and contributes significantly to the model’s parameter complexity. By integrating C-LoRA into the MLP block, we enable parameter-efficient updates that adapt to new tasks while preserving previously learned knowledge.

Low-Rank Adaptation in MLP: In a standard MLP block, the input features $\mathbf{x}_i \in \mathbb{R}^d$ are transformed as:

$$\text{MLP}(\mathbf{x}_i) = \sigma(\mathbf{x}_i \mathbf{W}_1 + \mathbf{b}_1) \mathbf{W}_2 + \mathbf{b}_2, \quad (18)$$

where $\mathbf{W}_1 \in \mathbb{R}^{d \times h}$ and $\mathbf{W}_2 \in \mathbb{R}^{h \times d}$ are the weight matrices, \mathbf{b}_1 and \mathbf{b}_2 are biases, and $\sigma(\cdot)$ is a non-linear activation function, such as ReLU. Directly updating these matrices for new tasks leads to significant parameter overhead and risks overwriting previously learned knowledge.

C-LoRA addresses these challenges by replacing full-rank updates with a low-rank adaptation mechanism. The modified MLP block operates by first projecting the input \mathbf{x}_i into a low-rank subspace using a down-sampling matrix $\mathbf{A} \in \mathbb{R}^{d \times r}$, where $r \ll d$. The intermediate representation is computed as:

$$\mathbf{z}_i = \sigma(\mathbf{x}_i \mathbf{A}), \quad (19)$$

where \mathbf{A} reduces the dimensionality of the input while preserving its essential features.

Routing Matrix and Task-Specific Updates: To facilitate continual learning, a routing matrix $\mathcal{R} \in \mathbb{R}^{r \times r}$ is introduced. This matrix is decomposed into two components:

$$\mathcal{R} = \mathcal{R}_{\text{old}} + \mathcal{R}_{\delta}, \quad (20)$$

where \mathcal{R}_{old} encodes knowledge from previously learned tasks and remains frozen during new task training, while \mathcal{R}_{δ} captures task-specific updates and is trainable for the current task.

The representation \mathbf{z}_i is modulated by both \mathcal{R}_{old} and \mathcal{R}_{δ} before being up-sampled back to the original dimensionality using $\mathbf{B} \in \mathbb{R}^{r \times d}$. The combined output is expressed as:

$$\text{C-LoRA}(\mathbf{x}_i) = \underbrace{\phi(\mathbf{z}_i \mathcal{R}_{\text{old}} \mathbf{B})}_{\text{stop-gradient for old}} + \underbrace{(\mathbf{z}_i \mathcal{R}_{\delta} \mathbf{B})}_{\text{update}}. \quad (21)$$

where $\phi(\cdot)$ is a stop-gradient operator that prevents \mathcal{R}_{old} from being updated during training. This mechanism ensures that shared knowledge is preserved while allowing flexibility for task-specific updates.

Integration into ViT: As shown in Figure 2, C-LoRA modifies the MLP block in ViT by combining its residual connection, original MLP computation, and the C-LoRA updates. The final output is computed as:

$$\text{out} = \mathbf{x}_i + \text{MLP}(\mathbf{x}_i) + \text{C-LoRA}(\mathbf{x}_i). \quad (22)$$

This formulation maintains the original representational power of the MLP block while incorporating task-specific adaptability through C-LoRA. Over successive tasks, the accumulated updates in \mathcal{R}_{δ} enable the model to adapt to new tasks without compromising performance on previously learned ones.

Loss Function Design: To mitigate catastrophic forgetting and promote stable learning across tasks, the total loss function combines a classification loss with an orthogonality regularization term:

$$\mathcal{L} = \mathcal{L}_{\text{ce}} + \lambda \mathcal{L}_{\text{orth}}, \quad (23)$$

where λ balances the contributions of the two terms.

The classification loss for incremental learning is defined as:

$$\mathcal{L}_{\text{ce}} = -\frac{1}{N_t} \sum_{j=1}^{N_t} \log \frac{\exp(z_{j,c^*})}{\sum_{\ell \in \mathcal{Y}(t)} \exp(z_{j,\ell})}, \quad (24)$$

where N_t is the total number of samples in the current task t ’s dataset, and $\mathcal{Y}(t)$ represents the set of class labels for the current task. The term

$$z_{j,\ell} = \frac{s(\mathbf{w}_{\ell}^{\top} \mathbf{f}_j)}{\|\mathbf{w}_{\ell}\| \|\mathbf{f}_j\|} \quad (25)$$

represents the scaled cosine similarity between the feature vector \mathbf{f}_j of sample j and the weight vector \mathbf{w}_{ℓ} of class ℓ , with s being a scaling factor to stabilize optimization. Here, $\mathbf{f}_j \in \mathbb{R}^d$ denotes the feature vector of the j -th sample, and $\mathbf{w}_{\ell} \in \mathbb{R}^d$ denotes the weight vector of class ℓ . Both vectors are

TABLE I

ACCURACY OF DIFFERENT CONTINUAL LEARNING METHODS ACROSS FOUR BENCHMARK DATASETS, EACH DIVIDED INTO 5 INCREMENTAL SESSIONS. THIS SETTING REFLECTS SCENARIOS WITH FEWER NEW CLASSES INTRODUCED PER SESSION, OFFERING INSIGHTS INTO PERFORMANCE STABILITY.

Method	Split CIFAR-100		Split ImageNet-A		Split CUB-200		Split CAR196	
	Last-Acc (%)	Inc-Acc (%)	Last-Acc (%)	Inc-Acc (%)	Last-Acc (%)	Inc-Acc (%)	Last-Acc (%)	Inc-Acc (%)
Joint-Training	93.22	-	79.61	-	90.78	-	68.66	-
EWC [53]	91.21 ± 0.53	93.93 ± 0.67	60.13 ± 2.28	68.74 ± 0.87	84.73 ± 0.74	91.07 ± 0.38	51.64 ± 1.36	61.47 ± 1.10
L2P [54]	84.60 ± 1.74	89.24 ± 1.27	46.94 ± 0.71	53.28 ± 1.13	73.07 ± 1.74	81.99 ± 1.34	56.03 ± 2.86	66.43 ± 2.40
DualPrompt [55]	82.66 ± 2.00	87.23 ± 0.88	50.54 ± 0.98	58.18 ± 1.30	74.28 ± 0.26	83.60 ± 0.44	48.90 ± 0.76	61.83 ± 0.44
LAE [56]	82.45 ± 0.49	87.11 ± 1.11	47.99 ± 0.91	56.29 ± 2.32	75.40 ± 0.99	84.77 ± 0.56	50.97 ± 0.96	62.46 ± 0.90
SLCA [47]	92.19 ± 0.56	94.56 ± 0.58	63.14 ± 1.39	68.65 ± 0.72	86.54 ± 1.27	91.51 ± 0.96	75.73 ± 1.27	82.01 ± 0.72
Adam+VPT-S [57]	84.10 ± 0.88	87.89 ± 1.49	24.49 ± 2.35	31.16 ± 1.73	86.64 ± 0.17	91.25 ± 0.14	30.86 ± 11.39	39.34 ± 13.77
Adam+VPT-D [57]	85.89 ± 4.11	89.41 ± 3.03	48.76 ± 4.90	56.59 ± 5.78	86.67 ± 0.13	91.23 ± 0.10	23.52 ± 13.70	30.80 ± 17.23
Adam+adapter [57]	88.63 ± 0.13	91.98 ± 0.85	49.79 ± 0.67	58.38 ± 1.33	87.25 ± 0.03	91.66 ± 0.23	40.75 ± 0.29	50.07 ± 1.81
Adam+ssf [57]	86.98 ± 0.26	90.91 ± 0.98	52.36 ± 1.53	61.08 ± 2.60	86.73 ± 0.05	91.18 ± 0.19	46.07 ± 0.66	55.58 ± 1.90
EASE [4]	89.33 ± 0.16	92.53 ± 0.92	62.92 ± 0.83	70.19 ± 1.18	83.93 ± 1.48	89.55 ± 0.84	54.98 ± 0.80	67.09 ± 1.08
Ours	92.17 ± 0.15	94.48 ± 0.79	63.84 ± 1.24	71.50 ± 1.34	90.55 ± 0.28	93.60 ± 0.30	78.70 ± 0.75	84.48 ± 0.94

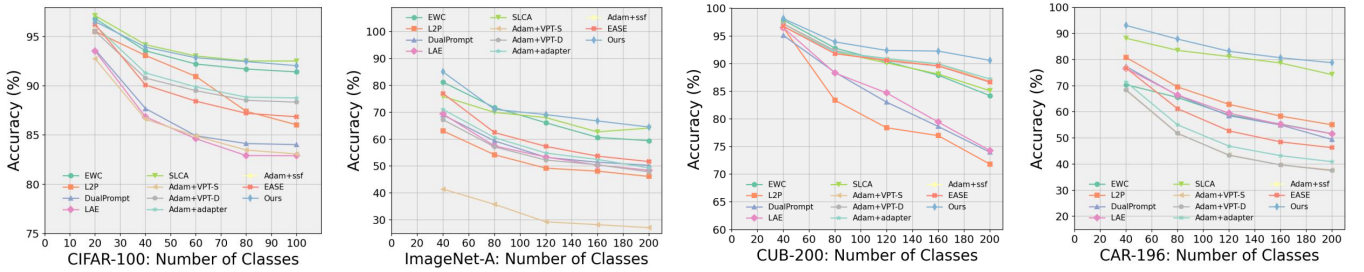


Fig. 3. Accuracy performance in each of the 5 incremental sessions on CIFAR-100, ImageNet-A, CUB-200, and CAR196.

normalized to ensure the similarity is computed based on their angular relationship. The numerator, $\exp(z_{j,c^*})$, quantifies the alignment between the feature vector and the weight vector of the correct class c^* , while the denominator aggregates the scaled similarities over all classes. This normalization ensures the logits are transformed into a probability distribution, allowing the model to focus on maximizing the likelihood of the correct class.

The orthogonality regularization ensures that task-specific updates in \mathcal{R}_δ do not interfere with the old parameter subspace by measuring \mathcal{R}_δ 's projection onto the low-rank subspace \mathbf{A}' of the old model:

$$\mathcal{L}_{\text{orth}} = \|(\mathbf{A}')^\top \mathcal{R}_\delta\|_F^2, \quad (26)$$

where \mathbf{A}' represents the current \mathbf{A} during the training process when a new task sample arrives, and $\|\cdot\|_F^2$ denotes the Frobenius norm.

In class-incremental learning scenarios, access to data from previous tasks is typically restricted. To address this, we employ a *feature resampling strategy* that generates synthetic features based on the statistical properties of each class. Specifically, we use the mean and covariance of features from each class to synthesize representative samples. This approach ensures that the model retains its discriminative power on old tasks without requiring direct access to their data.

IV. EXPERIMENTS

A. Experimental Setups

Datasets. Following previous studies [46]–[48], we evaluated our method on four benchmark datasets. CIFAR-100 [49]

consists of 100 classes with 60,000 images, approximately 50,000 for training (83%) and 10,000 for testing (17%). ImageNet-A [50] includes 200 classes and roughly 7,500 test samples. CUB-200 [51] contains 11,788 bird images across 200 subclasses, with about 6,000 for training (51%) and 5,800 for testing (49%). Car196 [52] comprises 196 car models with 16,185 images, split into around 8,150 for training (50%) and 8,035 for testing (50%).

Implementation Details. Following prior works [46], [47], we employ the pre-trained ViT-B/16-IN21K as the backbone network. During each training session, we use the SGD optimizer with a learning rate of 0.01, coupled with a cosine annealing scheduler starting at an initial value of 0.0005. The batch size is fixed at 48. The routing matrix \mathcal{R}_δ is initialized near zero at the start of each session, and we set the regularization parameter $\lambda = 0.01$ accordingly.

To evaluate performance, we calculate two metrics: “Last-Acc” and “Inc-Acc.” Last-Acc measures the average accuracy across all classes after the completion of the final task in the incremental learning process. Inc-Acc assesses the model’s performance throughout the entire incremental learning process by calculating the average accuracy across all tasks at the conclusion of each incremental learning phase. Specifically, for each task added during incremental learning, we compute the accuracy on all learned classes and take the average across all phases to obtain Inc-Acc. This metric provides a holistic view of the model’s ability to retain knowledge while learning new tasks, reflecting its robustness to catastrophic forgetting. To ensure robust comparisons, all experiments are conducted

TABLE II

ACCURACY OF DIFFERENT CONTINUAL LEARNING METHODS ACROSS FOUR BENCHMARK DATASETS, EACH DIVIDED INTO 10 INCREMENTAL SESSIONS.

Method	Split CIFAR-100		Split ImageNet-A		Split CUB-200		Split CAR196	
	Last-Acc (%)	Inc-Acc (%)	Last-Acc (%)	Inc-Acc (%)	Last-Acc (%)	Inc-Acc (%)	Last-Acc (%)	Inc-Acc (%)
Joint-Training	93.22	-	79.61	-	90.78	-	68.66	-
EWC [53]	90.59 ± 0.63	93.80 ± 0.97	56.24 ± 1.56	66.30 ± 1.71	85.10 ± 0.31	92.36 ± 0.51	45.58 ± 0.19	60.41 ± 0.94
L2P [54]	84.17 ± 0.91	88.20 ± 1.30	43.47 ± 0.89	50.52 ± 2.29	67.13 ± 2.03	79.62 ± 1.56	45.81 ± 0.98	57.85 ± 1.92
DualPrompt [55]	81.70 ± 1.07	86.42 ± 0.98	46.41 ± 0.20	55.95 ± 1.34	68.68 ± 0.35	80.75 ± 0.87	39.36 ± 2.32	53.93 ± 2.40
LAE [56]	87.53 ± 0.38	91.67 ± 1.04	60.74 ± 0.93	69.43 ± 1.31	81.55 ± 2.38	88.63 ± 1.84	44.07 ± 0.95	57.88 ± 1.12
SLCA [47]	91.07 ± 0.45	94.06 ± 1.07	58.96 ± 0.88	66.39 ± 2.16	84.55 ± 0.19	90.69 ± 0.65	66.49 ± 2.87	76.43 ± 0.61
Adam+VPT-S [57]	68.67 ± 12.40	75.22 ± 9.72	39.08 ± 9.51	49.08 ± 9.11	80.03 ± 11.42	86.60 ± 9.14	31.63 ± 10.15	41.78 ± 10.92
Adam+VPT-D [57]	84.61 ± 3.01	88.83 ± 2.70	37.00 ± 13.81	46.29 ± 14.94	86.73 ± 0.33	91.91 ± 0.15	38.04 ± 12.80	48.00 ± 14.05
Adam+adapter [57]	87.32 ± 0.28	91.21 ± 1.35	48.94 ± 0.10	58.95 ± 1.38	87.04 ± 0.13	92.13 ± 0.27	37.65 ± 0.09	49.22 ± 1.66
Adam+ssf [57]	85.26 ± 0.40	89.92 ± 0.84	49.60 ± 0.80	58.90 ± 2.22	86.32 ± 0.43	91.80 ± 0.55	42.83 ± 0.72	53.97 ± 1.94
EASE [4]	87.53 ± 0.38	91.67 ± 1.04	60.74 ± 0.93	69.43 ± 1.31	81.55 ± 2.38	88.63 ± 1.84	44.07 ± 0.95	57.88 ± 1.12
Ours	91.67 ± 0.05	94.29 ± 0.80	63.51 ± 0.78	71.88 ± 1.34	90.16 ± 0.15	93.87 ± 0.53	72.07 ± 1.12	80.42 ± 0.81

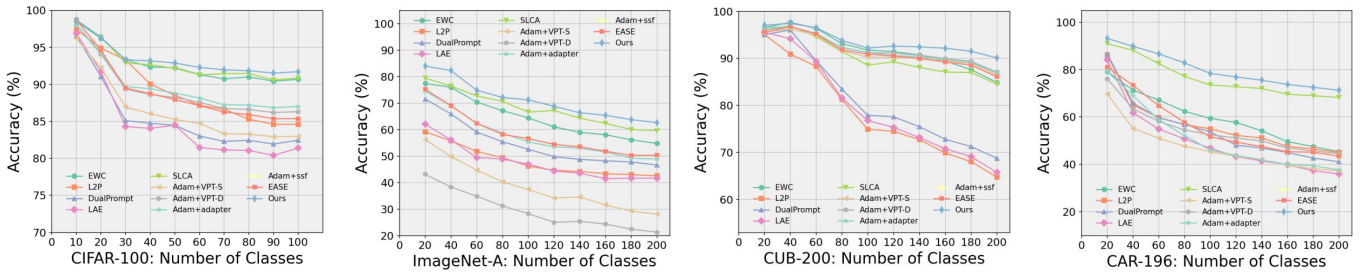


Fig. 4. Accuracy performance in each of the 10 incremental sessions on CIFAR-100, ImageNet-A, CUB-200, and CAR196.

using three fixed random seeds, and we report the mean and standard deviation of the results.

B. Evaluation Results Across Incremental Sessions

We evaluated the proposed method on four benchmark datasets under three incremental learning scenarios (5, 10, and 20 sessions). Table I, II, and III respectively present the performance for 5, 10, and 20 incremental sessions. Figures 3, 6, and 5 respectively illustrate the performance of our method on four datasets under 5, 10, and 20 incremental session settings. Each figure corresponds to a specific number of incremental sessions, with the datasets ordered from top to bottom as CIFAR-100, ImageNet-A, CUB-200, and CAR196. Our approach demonstrates strong adaptability and stability in handling diverse domain data and varying incremental settings, effectively mitigating catastrophic forgetting.

Our method consistently outperforms baseline approaches across datasets and session settings. For datasets with pre-training overlap, such as CIFAR-100 and CUB-200, our method achieves competitive Last-Acc and Inc-Acc scores with fewer parameter updates. For instance, on CIFAR-100, it achieves 91.67% Last-Acc and 94.29% Inc-Acc, matching or exceeding SLCA while requiring significantly less computation. On datasets with significant domain gaps, such as ImageNet-A and CAR196, our method demonstrates superior robustness. For example, on ImageNet-A, our approach achieves a Last-Acc of 63.51%, outperforming the second-best method by 4.14%. Similarly, it achieves a Last-Acc of 72.07% on CAR196, a 3.80% improvement over alternatives. Our method also exhibits remarkable stability across different

incremental scenarios. While catastrophic forgetting increasingly impacts other methods in longer sequences, our approach maintains consistent Last-Acc and Inc-Acc scores.

C. Ablation Study

To validate the effectiveness of each component in our proposed method, we conducted ablation experiments on the CUB-200 dataset, as shown in Table IV. The basic LoRA configuration exhibited a significant performance decline in 10 incremental tasks, achieving an Last-Acc of 81.21%, indicating that the module is susceptible to catastrophic forgetting without additional mechanisms.

We introduced the \mathcal{R} matrix to the basic LoRA configuration, denoted as LoRA+R, which resulted in improved Last-Acc of 82.49%, enabling efficient reuse of parameter subspaces. Next, we decomposed the \mathcal{R} matrix into \mathcal{R}_{old} and \mathcal{R}_{δ} , referred to as LoRA+R+TD. This enhanced the module’s retention and transfer capabilities across sessions, achieving Last-Acc of 90.09%. This modification facilitated the separation and independent adjustment of feature representations for old and new tasks.

Finally, we incorporated orthogonality constraints into the LoRA+R+TD configuration, resulting in C-LoRA, which further increased the Last-Acc to 90.30%. These results highlight the importance of orthogonality in mitigating catastrophic forgetting and maintaining feature space stability.

Figure 6 further report the effectiveness of the proposed components. The left shows accuracy changes over 10 incremental sessions. LoRA+R+TD outperforms both LoRA and LoRA+R, showing that our decomposition operation enhances

TABLE III
ACCURACY OF DIFFERENT CONTINUAL LEARNING METHODS ACROSS FOUR BENCHMARK DATASETS, EACH DIVIDED INTO 20 INCREMENTAL SESSIONS. THIS SETTING EMPHASIZES THE CHALLENGE OF LONGER TASK SEQUENCES, SHOWCASING THE RESILIENCE OF OUR APPROACH UNDER EXTENDED INCREMENTAL LEARNING.

Method	Split CIFAR-100		Split ImageNet-A		Split CUB-200		Split CAR196	
	Last-Acc (%)	Inc-Acc (%)	Last-Acc (%)	Inc-Acc (%)	Last-Acc (%)	Inc-Acc (%)	Last-Acc (%)	Inc-Acc (%)
Joint-Training	93.22	-	79.61	-	90.78	-	68.66	-
EWC 2017 [53]	89.96 ± 0.15	93.31 ± 1.02	54.62 ± 1.39	63.55 ± 1.53	87.25 ± 1.00	93.45 ± 0.48	44.42 ± 0.56	61.75 ± 1.06
L2P [54]	79.32 ± 1.49	84.10 ± 1.11	40.07 ± 1.42	49.35 ± 1.37	60.30 ± 3.80	73.53 ± 3.34	29.83 ± 3.31	42.82 ± 1.14
DualPrompt [55]	76.57 ± 0.60	82.97 ± 1.78	41.48 ± 1.63	52.84 ± 1.57	65.22 ± 1.29	77.86 ± 1.31	25.11 ± 2.09	40.89 ± 0.77
LAE [56]	75.40 ± 1.01	80.66 ± 0.70	32.28 ± 1.80	42.24 ± 2.53	56.73 ± 1.89	72.67 ± 1.14	19.62 ± 1.82	35.66 ± 3.32
SLCA [47]	90.37 ± 0.56	93.64 ± 0.99	53.76 ± 5.54	61.82 ± 4.74	82.37 ± 0.42	90.12 ± 0.93	56.09 ± 3.89	68.50 ± 2.42
Adam+VPT-S [57]	81.41 ± 1.00	86.48 ± 1.46	40.66 ± 5.37	51.32 ± 4.68	82.42 ± 5.75	89.46 ± 3.65	29.72 ± 8.31	41.08 ± 8.90
Adam+VPT-D [57]	73.60 ± 15.86	79.59 ± 13.27	37.07 ± 15.26	48.41 ± 15.17	86.67 ± 0.56	92.09 ± 0.87	36.76 ± 6.24	49.34 ± 7.03
Adam+adapter [57]	84.86 ± 0.29	89.41 ± 1.32	48.72 ± 0.07	59.53 ± 1.02	86.80 ± 0.02	92.42 ± 0.31	37.69 ± 0.02	50.56 ± 1.40
Adam+ssf [57]	82.96 ± 1.21	87.90 ± 0.05	47.86 ± 4.13	58.58 ± 4.27	86.37 ± 0.20	92.21 ± 0.63	41.98 ± 0.42	54.35 ± 1.29
EASE [4]	84.88 ± 1.09	90.08 ± 1.01	55.50 ± 1.16	65.73 ± 1.77	78.26 ± 1.02	87.14 ± 1.19	31.83 ± 1.38	47.90 ± 1.89
Ours	90.69 ± 0.25	93.57 ± 0.76	62.17 ± 0.86	70.00 ± 1.62	90.18 ± 0.11	94.11 ± 0.48	66.27 ± 0.68	75.85 ± 0.99

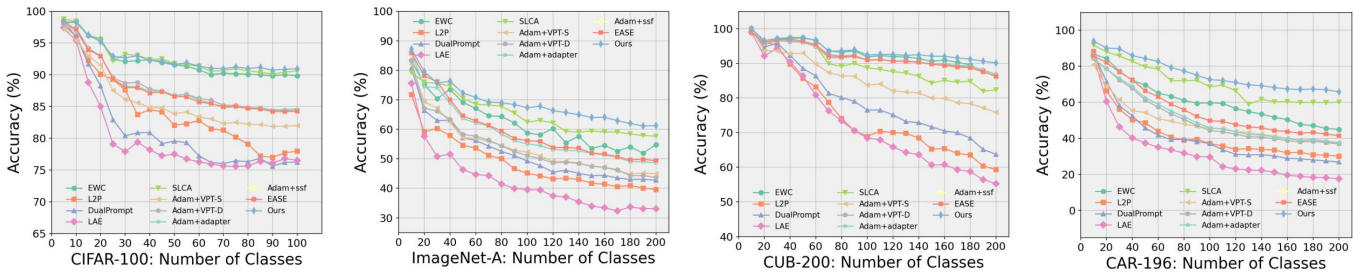


Fig. 5. Accuracy performance in each of the 20 incremental sessions on CIFAR-100, ImageNet-A, CUB-200, and CAR196.

TABLE IV
ABLATION RESULTS WITH DIFFERENT COMPONENTS ON CUB-200.

Method	Session1	Session2	Session3	Session4	Session5	Session6	Session7	Session8	Session9	Session10	Avg
LoRA	96.55	96.97	93.40	91.12	89.95	88.77	84.81	86.15	86.04	81.21	89.50
LoRA+R	96.55	96.74	93.85	90.79	88.82	90.00	85.73	87.05	86.98	82.49	89.90
LoRA+R+TD	97.04	97.44	96.40	93.50	92.46	92.90	92.34	92.38	91.51	90.09	93.61
C-LoRA	96.55	97.44	95.95	93.60	92.37	92.97	92.77	92.75	91.89	90.30	93.66

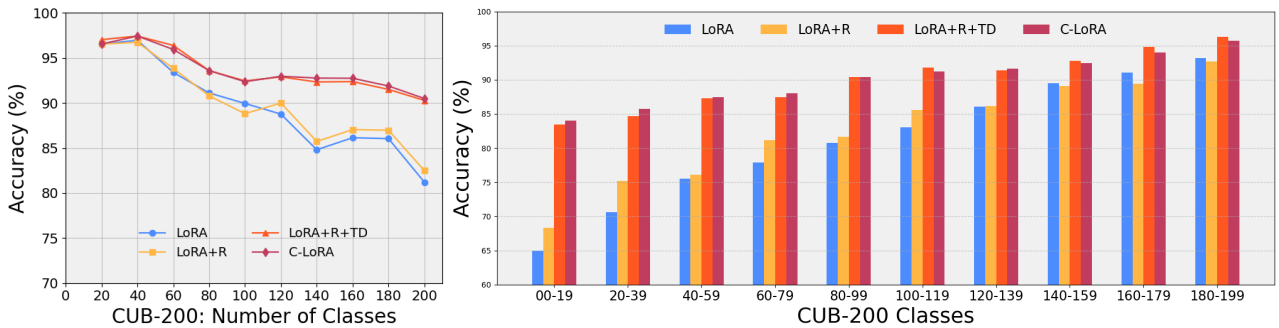


Fig. 6. (Left) Accuracy performance at each incremental session; (Right) Accuracy performance across different class intervals after incremental training.

continual learning. Although adding orthogonal loss results in a limited accuracy increase, it effectively reduces forgetting. The right presents accuracy across different class intervals after incremental training. As more training tasks are added, performance on older classes declines compared to newer ones. In contrast, our method maintains high accuracy on older tasks, showing the approach’s stability and performance improvements throughout the training process.

V. CONCLUSION

In summary, the proposed C-LoRA method effectively alleviates catastrophic forgetting and improves class-incremental learning performance across diverse datasets. Through multi-session scenarios and improved stability in our experiments, C-LoRA consistently delivers outstanding performance, surpassing existing approaches. Moreover, ablation studies underline the important role of the orthogonal low-rank adapter module,

providing robust empirical support for our design in class-incremental learning.

REFERENCES

- [1] E. J. Hu, Y. Shen, P. Wallis, Z. Allen-Zhu, Y. Li, S. Wang, L. Wang, and W. Chen, “Lora: Low-rank adaptation of large language models,” *arXiv preprint arXiv:2106.09685*, 2021.
- [2] M. Ayoub Kamal, M. M. Alam, A. A. B. Sajak, and M. Mohd Su’ud, “Requirements, deployments, and challenges of lora technology: A survey,” *Computational Intelligence and Neuroscience*, vol. 2023, no. 1, p. 5183062, 2023.
- [3] J. Yu, Y. Zhuge, L. Zhang, P. Hu, D. Wang, H. Lu, and Y. He, “Boosting continual learning of vision-language models via mixture-of-experts adapters,” in *Proceedings of the IEEE/CVF Conference on Computer Vision and Pattern Recognition*, 2024, pp. 23 219–23 230.
- [4] D.-W. Zhou, H.-L. Sun, H.-J. Ye, and D.-C. Zhan, “Expandable subspace ensemble for pre-trained model-based class-incremental learning,” in *Proceedings of the IEEE/CVF Conference on Computer Vision and Pattern Recognition*, 2024, pp. 23 554–23 564.
- [5] R. Aljundi, P. Chakraborty, and T. Tuytelaars, “Expert gate: Lifelong learning with a network of experts,” in *Proceedings of the IEEE conference on computer vision and pattern recognition*, 2017, pp. 3366–3375.
- [6] Z. Hu, Y. Li, J. Lyu, D. Gao, and N. Vasconcelos, “Dense network expansion for class incremental learning,” in *Proceedings of the IEEE/CVF Conference on Computer Vision and Pattern Recognition*, 2023, pp. 11 858–11 867.
- [7] J. L. McClelland, B. L. McNaughton, and R. C. O’Reilly, “Why there are complementary learning systems in the hippocampus and neocortex: insights from the successes and failures of connectionist models of learning and memory,” *Psychological review*, vol. 102, no. 3, p. 419, 1995.
- [8] R. M. French, “Catastrophic forgetting in connectionist networks,” *Trends in cognitive sciences*, vol. 3, no. 4, pp. 128–135, 1999.
- [9] M. McCloskey and N. J. Cohen, “Catastrophic interference in connectionist networks: The sequential learning problem,” in *Psychology of learning and motivation*. Elsevier, 1989, vol. 24, pp. 109–165.
- [10] A. Robins, “Catastrophic forgetting, rehearsal and pseudorehearsal,” *Connection Science*, vol. 7, no. 2, pp. 123–146, 1995.
- [11] G. I. Parisi, R. Kemker, J. L. Part, C. Kanan, and S. Wermter, “Continual lifelong learning with neural networks: A review,” *Neural networks*, vol. 113, pp. 54–71, 2019.
- [12] J. Dong, L. Wang, Z. Fang, G. Sun, S. Xu, X. Wang, and Q. Zhu, “Federated class-incremental learning,” in *Proceedings of the IEEE/CVF conference on computer vision and pattern recognition*, 2022, pp. 10 164–10 173.
- [13] J. Dong, D. Zhang, Y. Cong, W. Cong, H. Ding, and D. Dai, “Federated incremental semantic segmentation,” in *Proceedings of the IEEE/CVF Conference on Computer Vision and Pattern Recognition*, 2023, pp. 3934–3943.
- [14] Q. Gao, C. Zhao, B. Ghanem, and J. Zhang, “R-dfcil: Relation-guided representation learning for data-free class incremental learning,” in *European Conference on Computer Vision*. Springer, 2022, pp. 423–439.
- [15] D. Goswami, Y. Liu, B. Twardowski, and J. van de Weijer, “Fecam: Exploiting the heterogeneity of class distributions in exemplar-free continual learning,” *Advances in Neural Information Processing Systems*, vol. 36, 2024.
- [16] F.-Y. Wang, D.-W. Zhou, L. Liu, H.-J. Ye, Y. Bian, D.-C. Zhan, and P. Zhao, “Beef: Bi-compatible class-incremental learning via energy-based expansion and fusion,” in *The eleventh international conference on learning representations*, 2022.
- [17] H. Zhao, Y. Fu, M. Kang, Q. Tian, F. Wu, and X. Li, “Mgsvf: Multi-grained slow versus fast framework for few-shot class-incremental learning,” *IEEE Transactions on Pattern Analysis and Machine Intelligence*, vol. 46, no. 3, pp. 1576–1588, 2021.
- [18] Y. Liu, B. Schiele, and Q. Sun, “Rmm: Reinforced memory management for class-incremental learning,” *Advances in Neural Information Processing Systems*, vol. 34, pp. 3478–3490, 2021.
- [19] Z. Luo, Y. Liu, B. Schiele, and Q. Sun, “Class-incremental exemplar compression for class-incremental learning,” in *Proceedings of the IEEE/CVF Conference on Computer Vision and Pattern Recognition*, 2023, pp. 11 371–11 380.
- [20] Y. Wu, Y. Chen, L. Wang, Y. Ye, Z. Liu, Y. Guo, and Y. Fu, “Large scale incremental learning,” in *Proceedings of the IEEE/CVF conference on computer vision and pattern recognition*, 2019, pp. 374–382.
- [21] P. Buzzega, M. Boschini, A. Porrello, D. Abati, and S. Calderara, “Dark experience for general continual learning: a strong, simple baseline,” *Advances in neural information processing systems*, vol. 33, pp. 15 920–15 930, 2020.
- [22] L. Wang, X. Zhang, K. Yang, L. Yu, C. Li, L. Hong, S. Zhang, Z. Li, Y. Zhong, and J. Zhu, “Memory replay with data compression for continual learning,” *arXiv preprint arXiv:2202.06592*, 2022.
- [23] L. Wang, B. Lei, Q. Li, H. Su, J. Zhu, and Y. Zhong, “Triple-memory networks: A brain-inspired method for continual learning,” *IEEE Transactions on Neural Networks and Learning Systems*, vol. 33, no. 5, pp. 1925–1934, 2021.
- [24] S.-A. Rebuffi, A. Kolesnikov, G. Sperl, and C. H. Lampert, “icarl: Incremental classifier and representation learning,” in *Proceedings of the IEEE conference on Computer Vision and Pattern Recognition*, 2017, pp. 2001–2010.
- [25] P. Dhar, R. V. Singh, K.-C. Peng, Z. Wu, and R. Chellappa, “Learning without remembering,” in *Proceedings of the IEEE/CVF conference on computer vision and pattern recognition*, 2019, pp. 5138–5146.
- [26] A. Douillard, M. Cord, C. Ollion, T. Robert, and E. Valle, “Podnet: Pooled outputs distillation for small-tasks incremental learning,” in *Computer vision—ECCV 2020: 16th European conference, Glasgow, UK, August 23–28, 2020, proceedings, part XX 16*. Springer, 2020, pp. 86–102.
- [27] Z. Li and D. Hoiem, “Learning without forgetting,” *IEEE transactions on pattern analysis and machine intelligence*, vol. 40, no. 12, pp. 2935–2947, 2017.
- [28] C. Simon, P. Koniusz, and M. Harandi, “On learning the geodesic path for incremental learning,” in *Proceedings of the IEEE/CVF conference on Computer Vision and Pattern Recognition*, 2021, pp. 1591–1600.
- [29] X. Tao, X. Chang, X. Hong, X. Wei, and Y. Gong, “Topology-preserving class-incremental learning,” in *Computer Vision—ECCV 2020: 16th European Conference, Glasgow, UK, August 23–28, 2020, Proceedings, Part XIX 16*. Springer, 2020, pp. 254–270.
- [30] Y. Shi, K. Zhou, J. Liang, Z. Jiang, J. Feng, P. H. Torr, S. Bai, and V. Y. Tan, “Mimicking the oracle: An initial phase decorrelation approach for class incremental learning,” in *Proceedings of the IEEE/CVF conference on computer vision and pattern recognition*, 2022, pp. 16 722–16 731.
- [31] B. Zhao, X. Xiao, G. Gan, B. Zhang, and S.-T. Xia, “Maintaining discrimination and fairness in class incremental learning,” in *Proceedings of the IEEE/CVF conference on computer vision and pattern recognition*, 2020, pp. 13 208–13 217.
- [32] L. Wang, X. Zhang, Q. Li, M. Zhang, H. Su, J. Zhu, and Y. Zhong, “Incorporating neuro-inspired adaptability for continual learning in artificial intelligence,” *Nature Machine Intelligence*, vol. 5, no. 12, pp. 1356–1368, 2023.
- [33] B. Yang, X. Deng, H. Shi, C. Li, G. Zhang, H. Xu, S. Zhao, L. Lin, and X. Liang, “Continual object detection via prototypical task correlation guided gating mechanism,” in *Proceedings of the IEEE/CVF conference on computer vision and pattern recognition*, 2022, pp. 9255–9264.
- [34] Q. Zhou, X. Xiang, and J. Ma, “Hierarchical task-incremental learning with feature-space initialization inspired by neural collapse,” *Neural Processing Letters*, vol. 55, no. 8, pp. 10 811–10 827, 2023.
- [35] R. Aljundi, F. Babiloni, M. Elhoseiny, M. Rohrbach, and T. Tuytelaars, “Memory aware synapses: Learning what (not) to forget,” in *Proceedings of the European conference on computer vision (ECCV)*, 2018, pp. 139–154.
- [36] F. Zenke, B. Poole, and S. Ganguli, “Continual learning through synaptic intelligence,” in *International conference on machine learning*. PMLR, 2017, pp. 3987–3995.
- [37] X. Xiang, Y. Tan, Q. Wan, J. Ma, A. Yuille, and G. D. Hager, “Coarse-to-fine incremental few-shot learning,” in *European Conference on Computer Vision*. Springer, 2022, pp. 205–222.
- [38] S. Hayou, N. Ghosh, and B. Yu, “Lora+: Efficient low rank adaptation of large models,” *arXiv preprint arXiv:2402.12354*, 2024.
- [39] Y. Li, Y. Yu, C. Liang, P. He, N. Karampatziakis, W. Chen, and T. Zhao, “Loftq: Lora-fine-tuning-aware quantization for large language models,” *arXiv preprint arXiv:2310.08659*, 2023.
- [40] D. J. Kopiczko, T. Blankevoort, and Y. M. Asano, “Vera: Vector-based random matrix adaptation,” *arXiv preprint arXiv:2310.11454*, 2023.
- [41] X. Wei, G. Li, and R. Marculescu, “Online-lora: Task-free online continual learning via low rank adaptation,” *arXiv preprint arXiv:2411.05663*, 2024.

- [42] Y.-S. Liang and W.-J. Li, “Inflora: Interference-free low-rank adaptation for continual learning,” in *Proceedings of the IEEE/CVF Conference on Computer Vision and Pattern Recognition*, 2024, pp. 23 638–23 647.
- [43] R. A. Jacobs, M. I. Jordan, S. J. Nowlan, and G. E. Hinton, “Adaptive mixtures of local experts,” *Neural computation*, vol. 3, no. 1, pp. 79–87, 1991.
- [44] N. Shazeer, A. Mirhoseini, K. Maziarz, A. Davis, Q. Le, G. Hinton, and J. Dean, “Outrageously large neural networks: The sparsely-gated mixture-of-experts layer,” *arXiv preprint arXiv:1701.06538*, 2017.
- [45] D. Alexey, “An image is worth 16x16 words: Transformers for image recognition at scale,” *arXiv preprint arXiv: 2010.11929*, 2020.
- [46] M. D. McDonnell, D. Gong, A. Parvaneh, E. Abbasnejad, and A. van den Hengel, “Ranpac: Random projections and pre-trained models for continual learning,” *Advances in Neural Information Processing Systems*, vol. 36, 2024.
- [47] G. Zhang, L. Wang, G. Kang, L. Chen, and Y. Wei, “Slca: Slow learner with classifier alignment for continual learning on a pre-trained model,” in *Proceedings of the IEEE/CVF International Conference on Computer Vision*, 2023, pp. 19 148–19 158.
- [48] Y. Tan, Q. Zhou, X. Xiang, K. Wang, Y. Wu, and Y. Li, “Semantically-shifted incremental adapter-tuning is a continual vitransformer,” in *Proceedings of the IEEE/CVF Conference on Computer Vision and Pattern Recognition*, 2024, pp. 23 252–23 262.
- [49] A. Krizhevsky, G. Hinton *et al.*, “Learning multiple layers of features from tiny images.(2009),” 2009.
- [50] D. Hendrycks, K. Zhao, S. Basart, J. Steinhardt, and D. Song, “Natural adversarial examples,” in *Proceedings of the IEEE/CVF conference on computer vision and pattern recognition*, 2021, pp. 15 262–15 271.
- [51] C. Wah, S. Branson, P. Welinder, P. Perona, and S. Belongie, “The caltech-ucsd birds-200-2011 dataset,” 2011.
- [52] J. Krause, M. Stark, J. Deng, and L. Fei-Fei, “3d object representations for fine-grained categorization,” in *Proceedings of the IEEE international conference on computer vision workshops*, 2013, pp. 554–561.
- [53] J. Kirkpatrick, R. Pascanu, N. Rabinowitz, J. Veness, G. Desjardins, A. A. Rusu, K. Milan, J. Quan, T. Ramalho, A. Grabska-Barwinska *et al.*, “Overcoming catastrophic forgetting in neural networks,” *Proceedings of the national academy of sciences*, vol. 114, no. 13, pp. 3521–3526, 2017.
- [54] Z. Wang, Z. Zhang, C.-Y. Lee, H. Zhang, R. Sun, X. Ren, G. Su, V. Perot, J. Dy, and T. Pfister, “Learning to prompt for continual learning,” in *Proceedings of the IEEE/CVF conference on computer vision and pattern recognition*, 2022, pp. 139–149.
- [55] Z. Wang, Z. Zhang, S. Ebrahimi, R. Sun, H. Zhang, C.-Y. Lee, X. Ren, G. Su, V. Perot, J. Dy *et al.*, “Dualprompt: Complementary prompting for rehearsal-free continual learning,” in *European Conference on Computer Vision*. Springer, 2022, pp. 631–648.
- [56] Q. Gao, C. Zhao, Y. Sun, T. Xi, G. Zhang, B. Ghanem, and J. Zhang, “A unified continual learning framework with general parameter-efficient tuning,” in *Proceedings of the IEEE/CVF International Conference on Computer Vision*, 2023, pp. 11 483–11 493.
- [57] D.-W. Zhou, Z.-W. Cai, H.-J. Ye, D.-C. Zhan, and Z. Liu, “Revisiting class-incremental learning with pre-trained models: Generalizability and adaptivity are all you need,” *arXiv preprint arXiv:2303.07338*, 2023.